



**HAL**  
open science

## Defining the Upper Nisyros Pumice ( $57.1 \pm 1.5$ ka) as new tephra isochrone for linking early MIS-3 palaeoenvironmental records in the Aegean-Black Sea gateway: New evidence from the Sea of Marmara

Sabine Wulf, M Namik Çağatay, Oona Appelt, K Kadir Eriş, Pierre Henry

### ► To cite this version:

Sabine Wulf, M Namik Çağatay, Oona Appelt, K Kadir Eriş, Pierre Henry. Defining the Upper Nisyros Pumice ( $57.1 \pm 1.5$  ka) as new tephra isochrone for linking early MIS-3 palaeoenvironmental records in the Aegean-Black Sea gateway: New evidence from the Sea of Marmara. *Quaternary Science Reviews*, 2021, 274, pp.107285. 10.1016/j.quascirev.2021.107285 . hal-03462656

**HAL Id: hal-03462656**

**<https://hal.science/hal-03462656>**

Submitted on 2 Dec 2021

**HAL** is a multi-disciplinary open access archive for the deposit and dissemination of scientific research documents, whether they are published or not. The documents may come from teaching and research institutions in France or abroad, or from public or private research centers.

L'archive ouverte pluridisciplinaire **HAL**, est destinée au dépôt et à la diffusion de documents scientifiques de niveau recherche, publiés ou non, émanant des établissements d'enseignement et de recherche français ou étrangers, des laboratoires publics ou privés.



Distributed under a Creative Commons Attribution - NonCommercial - NoDerivatives 4.0 International License

1 **Defining the Upper Nisyros Pumice ( $57.1 \pm 1.5$  ka) as new tephra isochrone for**  
2 **linking early MIS-3 palaeoenvironmental records in the Aegean-Black Sea**  
3 **region: new evidence from the Sea of Marmara**

4 Sabine Wulf<sup>1\*</sup>, M. Namık Çağatay<sup>2</sup>, Oona Appelt<sup>3</sup>, K. Kadir Eriş<sup>2</sup>, and Pierre Henry<sup>4</sup>

5 <sup>1</sup> School of the Environment, Geography and Geosciences, University of Portsmouth, Lion  
6 Terrace, Portsmouth, PO1 3HE, United Kingdom

7 <sup>2</sup> İstanbul Technical University, EMCOL Research Centre and Department of Geological  
8 Engineering, Ayazağa, 34469, İstanbul, Turkey

9 <sup>3</sup> Helmholtz Centre Potsdam, GFZ German Research Centre of Geosciences, Section 3.6,  
10 Telegrafenberg, 14473 Potsdam, Germany

11 <sup>4</sup> CEREGE (UMR7330), Aix-Marseille Université, CNRS-IRD, 13330, Marseille 7, France

12 \*Corresponding author: [sabine.wulf@port.ac.uk](mailto:sabine.wulf@port.ac.uk) (S. Wulf)

13

14 **Keywords:** Cryptotephra, Upper Nisyros Pumice, Sea of Marmara, Eastern Mediterranean

15 **Abstract**

16 The rhyolitic Upper Nisyros Pumice (UNP) from the Kos-Yali-Nisyros volcanic system has  
17 been detected as a cryptotephra layer in lacustrine sediments from the Sea of Marmara (SoM).  
18 A new independent age of the UNP eruption at  $57.1 \pm 1.5$  cal ka BP has been interpolated  
19 using a combination of radiocarbon dating, tephrochronology and wiggle-matching of the SoM  
20 proxy record (Ca-curves) with Greenland oxygen isotope data, therewith confirming recently  
21 published radioisotopic dates of UNP land deposits. The UNP tephra in the SoM was identified  
22 by comparisons of the SoM tephra glass chemical dataset with published data of other marine  
23 tephra records from the Aegean Sea and the Megali Limni lacustrine sediment sequence  
24 (Lesvos Island). The stratigraphic position of the UNP tephra in these records verified its  
25 deposition in the SoM at the onset of MIS-3 and specifically at the termination of Greenland  
26 Interstadial GI-16. The new findings define the UNP tephra as a valuable time marker for the  
27 synchronisation of palaeoenvironmental data for this time period and help spurring the

28 establishment of a robust tephrostratigraphical framework for the last ~70 kyr in the Aegean-  
29 Black Sea region.

## 30 **1. Introduction**

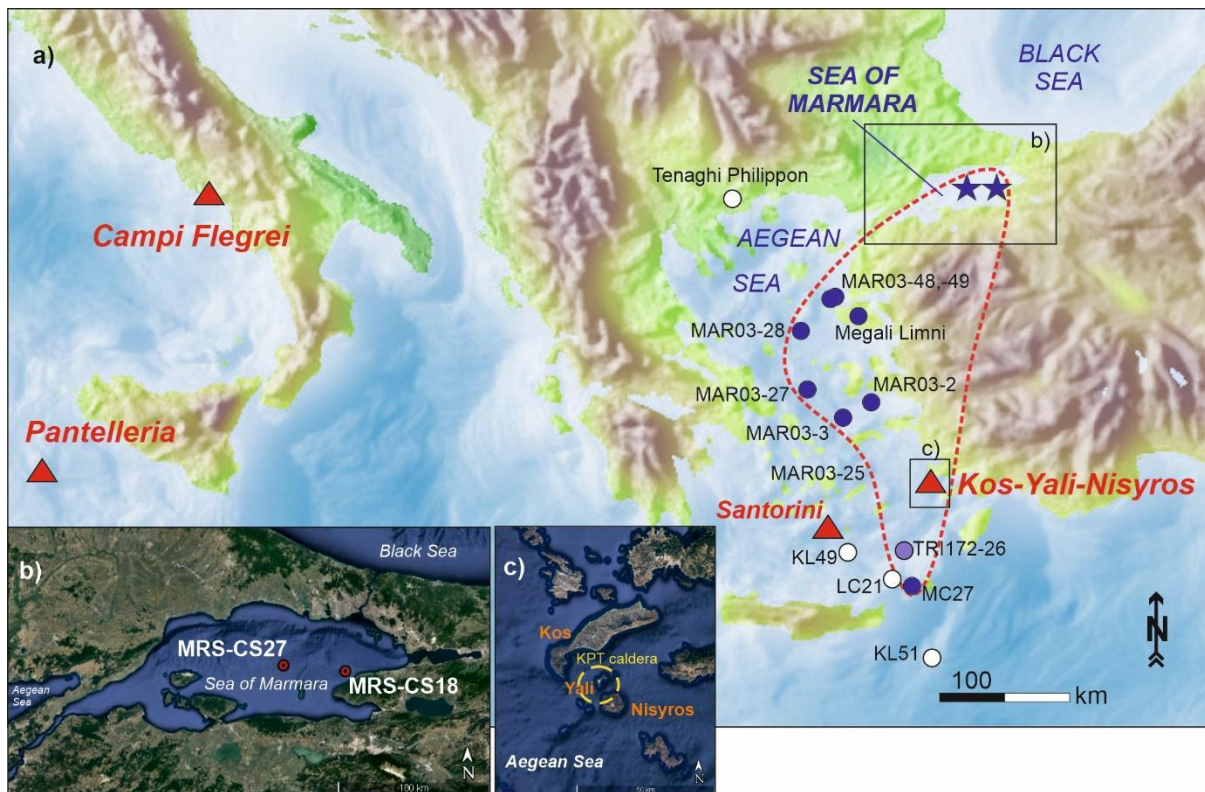
31 Tephra layers in sedimentary records have been well established as tools for dating and  
32 synchronizing palaeoclimate and -environmental data (e.g., Lowe, 2011), with numerous  
33 examples derived from European records. Those include records from the Eastern  
34 Mediterranean region which is characterised by intense and frequent explosive volcanic  
35 activity (e.g., Italian and Aegean Arc volcanoes) and widespread tephra dispersal (e.g., Keller  
36 et al., 1978; Narcisi and Vezzoli, 1999; Bourne et al., 2015; Satow et al., 2015; Giaccio et al.,  
37 2012, 2019; Wulf et al., 2012, 2018, 2020; Vakhrameeva et al., 2018, 2019). To date,  
38 numerous tephra markers from Italian volcanoes have been established as reliable isochrones  
39 that provide precise and accurate absolute dates of the timing of their eruption (e.g., Giaccio  
40 et al., 2012, 2017, 2019). However, dating of calc-alkaline tephra from Aegean Arc volcanoes  
41 (e.g., Milos, Santorini, Kos, Nisyros, Yali) still lack absolute dating, mainly because advanced  
42 radioisotopic dating techniques such as  $^{40}\text{K}/^{40}\text{Ar}$  or  $^{40}\text{Ar}/^{39}\text{Ar}$  are not suitable (e.g., Druitt et al.,  
43 1999; Fabbro et al., 2013). One approach to overcome those dating problems is to interpolate  
44 tephra deposition ages from sediment core chronologies of distal archives, as recently  
45 demonstrated for Santorini tephra layers in Aegean Sea records (e.g., Satow et al., 2015,  
46 2020; Wulf et al., 2020).

47 Compared to Santorini, the calc-alkaline Kos-Yali-Nisyros (KYN) magmatic system in the SE  
48 part of the Aegean Sea still lacks a detailed tephrostratigraphy. Volcanic activity at the KYN  
49 started approximately 3 Ma ago (Bachmann et al., 2010). One of the largest, caldera-forming  
50 eruption occurred at  $161.3 \pm 1.1$  ka resulting in the widespread dispersal of the Kos Plateau  
51 Tuff (KPT; e.g., Smith et al., 1996; Hardiman, 1999; Allen, 2001). Subsequently, the volcanic  
52 centres of Nisyros and Yali formed within the KPT caldera (Figs. 1a, c), which produced

53 several large explosive eruptions during the last 160 kyr (e.g., Pe-Piper and Moulton, 2008;  
54 Bachmann et al., 2012).

55 Nisyros activities in particular were characterised by alternating effusive and explosive cycles  
56 that erupted calc-alkaline basaltic-andesitic to rhyolitic lavas and pyroclastics (e.g., Di Paola,  
57 1974; Limburg and Varekamp, 1991; Longchamp et al., 2011; Tomlinson et al., 2012a). Two  
58 major Plinian, caldera-forming events, the Lower (LNP) and Upper Nisyros Pumice (UNP)  
59 eruptions, formed massive tephra deposits on land and ash layers in distal terrestrial (Margari  
60 et al., 2007) and marine (e.g., Vinci, 1985; Hardiman, 1999; Aksu et al., 2008) settings. The  
61 timing of the LNP and UNP eruptions were controversially constrained to 110 - 28 ka (LNP;  
62 Rehren, 1988; Barberi et al., 1988; Hardiman, 1999; Aksu et al., 2008) and >50 - 35 ka (UNP;  
63 Vinci, 1985; Limburg and Varekamp, 1991; Margari et al., 2007; Karkanias et al., 2015),  
64 prohibiting for a long time the use of these tephra as reliable isochrones. However, recent  
65 advances in U-Th disequilibrium dating of zircon crystals have provided first absolute ages for  
66 the LNP and UNP eruptions at  $63.1 \pm 4.7$  ka and  $58.4 \pm 2.7$  ka respectively (Popa et al., 2020);  
67 those, however, still need verification by other independent dating techniques.

68 In this study, a comprehensive tephra glass chemical dataset and sediment accumulation rate  
69 age interpolation of a cryptotephra layer in sediments from the Sea of Marmara (SoM) is used  
70 to establish robust correlation and independent age control for the UNP eruption. The new  
71 dataset is used to re-evaluate previously published distal tephra findings in the Eastern  
72 Mediterranean region, with special focus on Nisyros tephra findings in the Megali Limni  
73 lacustrine sequence from Lesvos (Margari et al., 2007, 2009) and in Aegean Sea cores (Aksu  
74 et al., 2008; İşler et al., 2016). The results will help to develop a more robust  
75 tephrostratigraphical framework in the Aegean-Black Sea region for the last 70 kyr.



78 **Figure 1:** a) Topographic map of the Eastern Mediterranean depicting the coring locations of  
 79 MRS-CS18 and MRS-CS27 (blue stars) from the Sea of Marmara in relation to relevant  
 80 volcanic provinces (red triangles) and other marine and terrestrial archives (blue dots) with  
 81 Upper Nisyros Pumice occurrences. Tephra data are retrieved from Aksu et al. (2008) (MAR  
 82 sites), Vinci (1985) (site MC27), Hardiman (1999) (purple site TRI172-26 with undefined  
 83 Nisyros tephra occurrence), and Margari et al. (2007, 2009) (Megali Limni). White dots depict  
 84 sites that lack Nisyros tephra (Tenaghi Philippon, Wulf et al., 2018; LC21, Satow et al., 2015;  
 85 KL49, KL51, Wulf et al., 2020). The red dotted line indicates the proposed dispersal area of  
 86 the UNP (this study). b) GoogleEarth inlet map showing the detailed positions of cores MRS-  
 87 CS18 and MRS-C27 in the SoM (red dots). c) GoogleEarth inlet map of the Kos-Yali-Nisyros  
 88 volcanic complex with the inferred KPT caldera (dotted yellow line).

## 89 2. Material and methods

90 Sediment cores used in this study derived from the central and eastern part of the SoM. The  
 91 SoM is a brackish water basin in the Eastern Mediterranean region that connects the saline  
 92 Aegean Sea and the Black Sea brackish water basin via the Dardanelles and Bosphorus straits  
 93 (Figs. 1a, b). Cores MRS-CS18 and MRS-CS27 were retrieved in 2015 on board of the RV

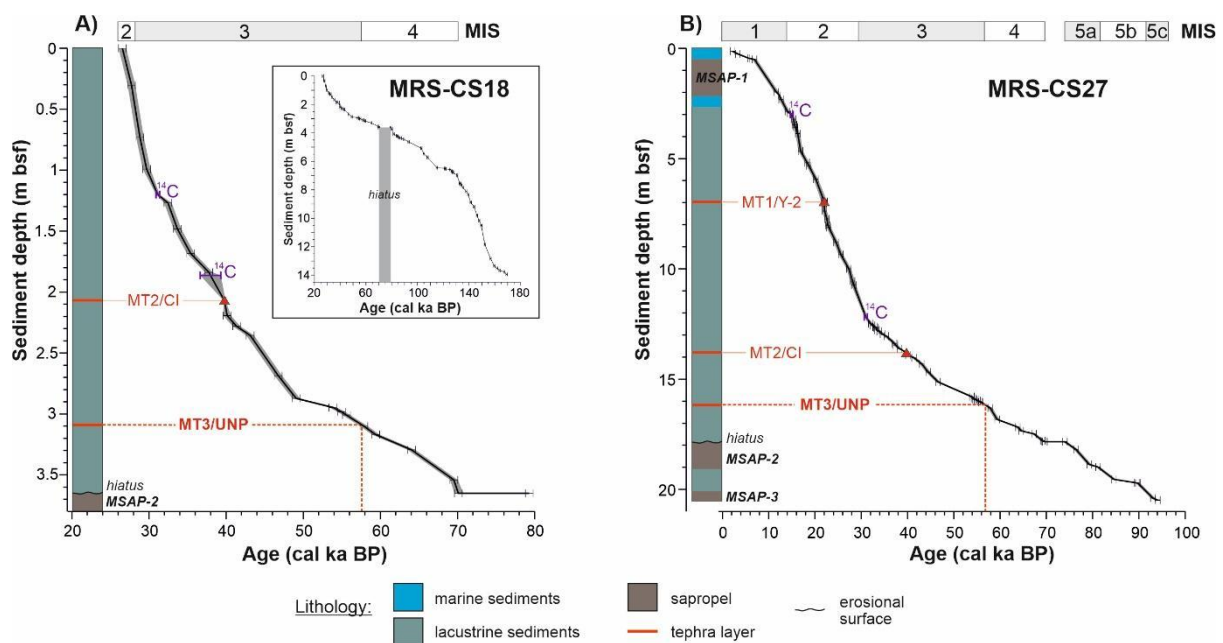
94 Pourquoi pas? from 291 m below sea level (b.s.l.) and 313 m b.s.l. at the northeastern and  
95 western edges of the İmrâli Basin in the SoM, respectively (Çağatay et al., 2019) (Fig. 1b).  
96 Sediments of both cores encompass alternating lacustrine and marine facies interrupted by a  
97 hiatus (Fig. 2) which indicates past major water level variations (Çağatay et al., 2019). Core  
98 MRS-CS18 is a 14.05 m long sequence that contains an 8-cm-thick brown tephra layer (CS18-  
99 MT2) at 2.03-2.11 mbsf and a 2-mm-thin ash layer (CS18-MT3) at 3.095 mbsf. Core MRS-  
100 CS27 comprises a 20.45 m long sediment sequences that shows three distinct tephra layers:  
101 the greyish CS27-MT1 (6.955-7.005 mbsf), the brownish CS27-MT2 (13.835-13.88 mbsf), and  
102 the mm-thin CS27-MT3 ash layer at 16.18 mbsf. Based on their similar stratigraphic positions  
103 and appearances in other SoM cores (Çağatay et al., 2015) the thick MT1 and MT2 tephra  
104 layers have been tentatively correlated to the Y-2/Cape Riva eruption of Santorini and the Y-  
105 5/Campanian Ignimbrite by Çağatay et al. (2019). The MT3 ash layer has been detected in  
106 cores MRS-CS18 and MRS-CS27 by studying sections of increased values in magnetic  
107 susceptibility and XRF-Calcium counts of sediments. Çağatay et al. (2019) roughly associated  
108 the MT-3 tephra with the marine X-1 tephra based on its chronostratigraphic position in both  
109 cores below the Campanian Ignimbrite (Çağatay et al., 2019). However, all these tentative  
110 tephra assignments still require verification by glass geochemical fingerprinting.

111 In this study, polished thin sections of tephra glass concentrate of the five tephra layers in  
112 cores MRS-CS18 (MT2, MT3) and MRS-CS27 (MT1, MT2, MT3) were used to determine the  
113 major element compositions of individual glass shards by electron probe microanalyses  
114 (Supplement A). Measurements were carried out at the GFZ Potsdam (Germany) using a  
115 JEOL-JXA8230 (WDS) probe with the following analytical setup: 15 kV accelerating voltage,  
116 10 nA beam current and 8-10  $\mu\text{m}$  beam size. Analytical count times were 20 seconds for the  
117 elements Fe, Mn, Ti, Mg, P, and Cl, and 10 seconds for elements Si, Al, K, Ca, and Na  
118 measured first. The natural Lipari obsidian (Hunt and Hill, 1996; Kuehn et al., 2011) and  
119 artificial glass standards from the Max Planck Institute (MPI-glasses: ATHO-G, StHs6/80 and  
120 GOR-132; Jochum et al., 2006) were used for data quality insurance (Supplement A).

121 Correlation of MT tephras used bivariate elemental plots of MT glass data and published glass  
122 datasets (Fig. 3).

123 MT3 tephra ages in SoM cores have been constrained by slightly revising the original age-  
124 depth models of cores MRS-CS18 and MRS-CS27 (Çağatay et al., 2019), which are based  
125 on a combination of wiggle-matching of the XRF-Ca-curves of both cores with interstadials of  
126 the NGRIP oxygen isotope curve (Andersen et al., 2006; Svensson et al., 2008; Wolff et al.,  
127 2010), radiocarbon dates on fossil shell samples, and tephrochronology (Fig. 2, Supplement  
128 A, Supplement Fig. B1). The revised sediment chronologies used the newest INTCAL20  
129 version by Reimer et al. (2020) for radiocarbon age calibration as well as up-to-date published  
130 tephra ages (Supplement Table B1). Tephra ages were calculated as average values from the  
131  $2\sigma$  age ranges that were obtained by Bayesian modelling using the OxCal version 4.4.3 (Bronk  
132 Ramsey, 2021) (Supplement A). The revision of the original chronology of the Megali Limni  
133 lacustrine sequence ML01 (Margari et al., 2007, 2009) to estimate ages of potential Nisyros  
134 tephra equivalents used the same approach (see details in Supplement Fig. B2, Supplement  
135 C).

136



138

139 **Figure 2:** Lithologies and age-depth models of Sea of Marmara cores MRS-CS18 **(a)** and  
140 MRS-CS27 **(b)** for the interval of the last 70 kyr. The inlet graph (a) depicts the complete  
141 chronology of core MRS-CS18 as described in Çağatay et al. (2019). Core chronologies are  
142 based on a combination of radiocarbon dates (purple bars), imported tephra ages (red  
143 triangles) and wiggle-matching with the NGRIP oxygen isotope record (black bars). The  
144 MT3/UNP tephra ages (red dotted lines) derive from Bayesian modelling (Supplement A).  
145 MSAP represents typical sapropel layers in the Sea of Marmara, after marine re-connections  
146 during the interglacial periods.

### 147 **3. Results**

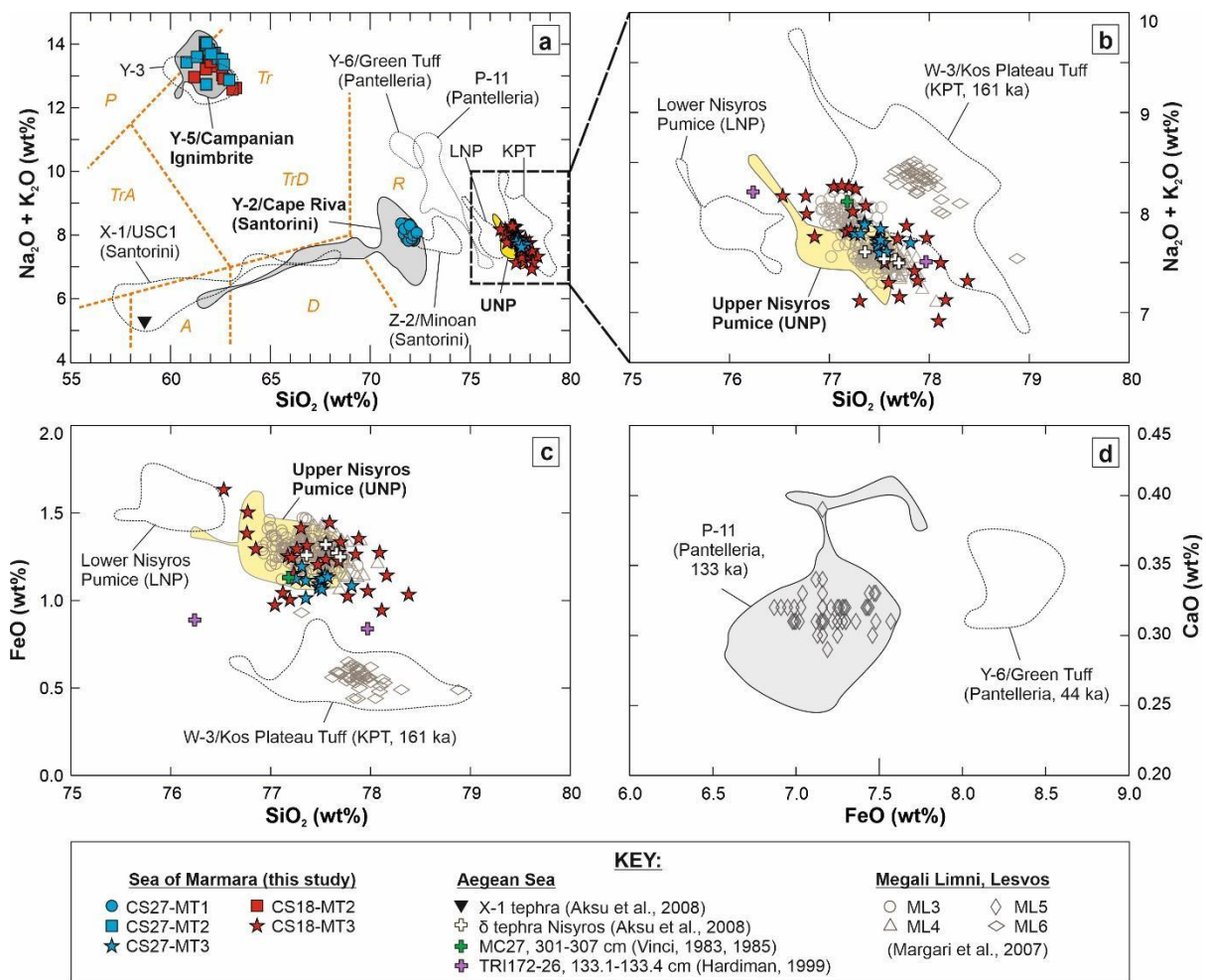
148 Tephrae MT1 and MT2 in both SoM cores have rhyolitic and phono-trachytic major element  
149 glass compositions that confirm the proposed correlation by Çağatay et al. (2019) to the Y-  
150 2/Cape Riva and Y-5/Campanian Ignimbrite tephrae, respectively (Fig. 3a, Supplement A).  
151 Therefore, the published eruption ages for the Y-2 ( $22.02 \pm 0.64$  cal ka BP; Bronk Ramsey et  
152 al., 2015) and Y-5 tephrae ( $39.85 \pm 0.14$   $^{40}\text{Ar}/^{39}\text{Ar}$  ka,  $39.78 \pm 0.14$  cal a BP; Giaccio et al.,  
153 2017) were implemented as independent time markers for the construction of the revised age-  
154 depth models (Fig. 2).

155 The glass composition of the MT3 cryptotephra layer is high-silica rhyolitic with concentration  
156 ranges in  $\text{SiO}_2$  of 76.5-78.4 wt%,  $\text{Al}_2\text{O}_3$  of 11.9-12.6 wt%, FeO of 0.6-1.6 wt%, CaO of 0.7-1.2  
157 wt%,  $\text{K}_2\text{O}$  of 3.6-4.9 wt%, and total alkalis ( $\text{Na}_2\text{O}+\text{K}_2\text{O}$ ) of 7.1-8.3 wt% (normalised data)  
158 (Supplement A). This major element glass chemistry is typical for tephrae from the eastern  
159 Aegean Arc and particularly from the Kos-Yali-Nisyros volcanic system. The MT3 glass  
160 chemistry clearly matches the glass composition of the proximal deposits of the Upper Nisyros  
161 Pumice (Tomlinson et al., 2012a), which can be well discriminated from the Lower Nisyros  
162 Pumices (LNP) by slightly higher mean values in  $\text{SiO}_2$  (77.2 vs. 76.1 wt%) and lower  
163 concentrations in  $\text{Al}_2\text{O}_3$  (12.3 vs. 12.9 wt%), FeO (1.3 vs. 1.5 wt%) and  $\text{Na}_2\text{O}$  (3.3 vs. 3.7 wt%)  
164 (Figs. 3b-c).



165 The timing of the MT3 tephra deposition in the SoM has been interpolated by the  
 166 revised age-depth models of the MRS-CS18 and MRS-CS27 cores at  $57,440 \pm 1570$  cal a BP  
 167 and  $56,710 \pm 1420$  cal a BP, respectively (Fig. 2). The mean age yields at  $57,080 \pm 1,500$  cal  
 168 a BP, which agrees well within its  $2\sigma$  uncertainty with the U-Th disequilibrium (zircon) age of  
 169 the proximal Upper Nisyros Pumice deposits at  $58.4 \pm 2.7$  ka BP obtained by Popa et al.  
 170 (2020). Furthermore, the chronostratigraphic position of the MT3 tephra as inferred from  
 171 wiggle-matching of the SoM Ca-curves with Greenland isotope data suggests a deposition in  
 172 both cores at the termination of Greenland Interstadial GI-16 (Fig. 4b-c).

173



174

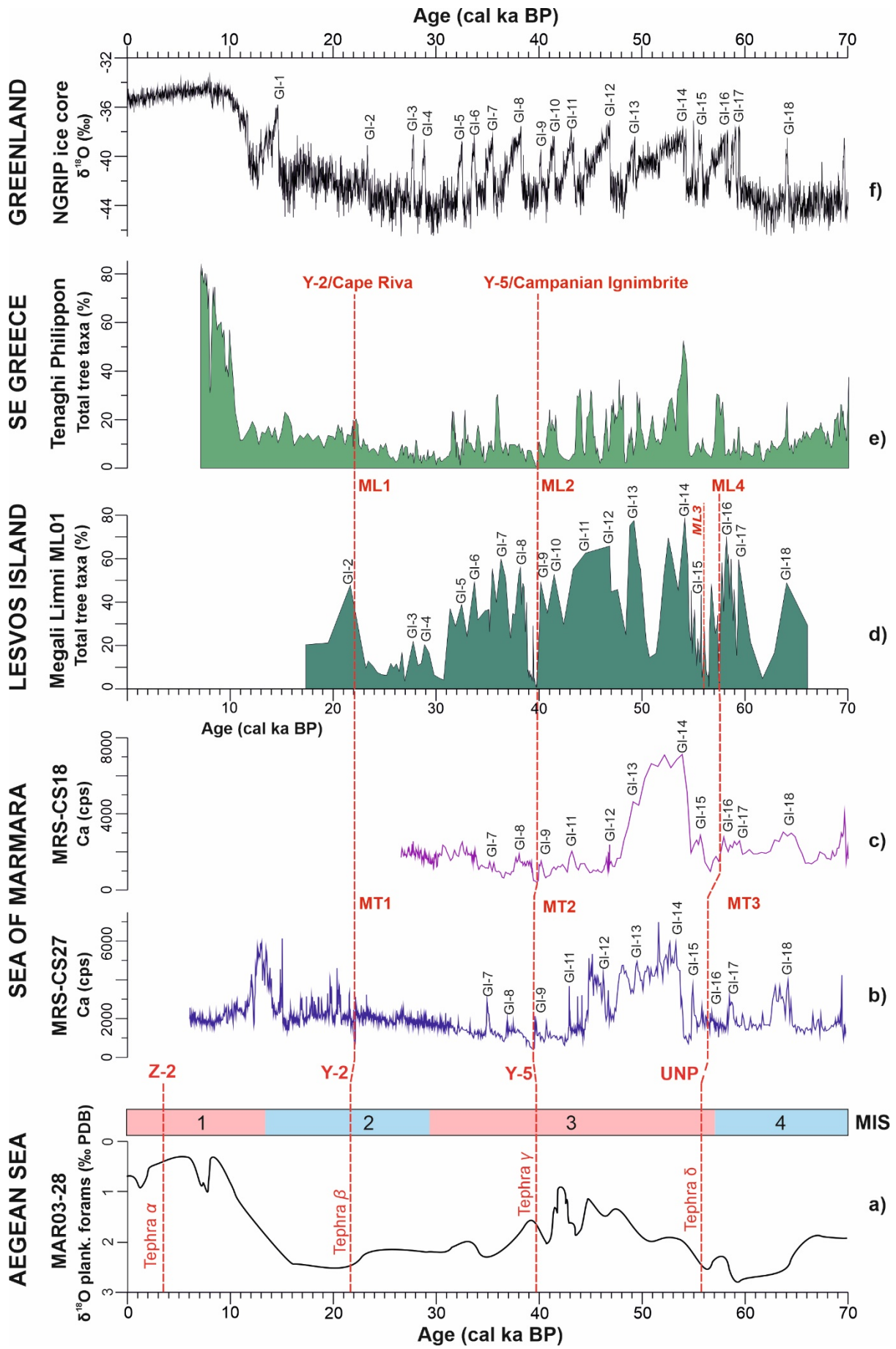
175 **Figure 3: (a-d)** Bivariate elemental plots of glass compositions of MT tephras of the Sea of  
 176 Marmara cores (this study), compared with published tephra datasets (envelopes) and  
 177 potential distal correlatives from the Aegean Sea (Aksu et al., 2008; Vinci, 1983, 1985;

178 Hardiman, 1999) and Megali Limni, Lesvos Island, Greece (Margari et al., 2007). Tephra glass  
179 chemical datasets are retrieved from: *Z-2/Minoan and Y-2/Cape Riva*: Kwiecien et al. (2008),  
180 Tomlinson et al. (2015), Wulf et al. (2018, 2020); *Y-3*: Albert et al. (2015), Wulf et al. (2018,  
181 2020); *Y-5/Campanian Ignimbrite*: Tomlinson et al. (2012b), Wulf et al. (2018); *Y-6/Green Tuff*:  
182 Tomlinson et al. (2015); *X-1/Upper Scoriae 1*: Wulf et al. (2020); *P-11*: Satow et al. (2015),  
183 Vogel et al. (2010), Leicher et al. (2016); *Lower and Upper Nisyros Pumice (LNP, UNP)*:  
184 Tomlinson et al. (2012a); *W-3/Kos Plateau Tuff*: Satow et al. (2015), Wegwerth et al. (2019),  
185 Wulf et al. (2020).

#### 186 **4. Discussion**

187 The comparison with distal tephra datasets shows that the MT3 tephra from the SoM  
188 correlates with the rhyolitic tephra  $\delta$  identified in several Aegean Sea cores (Aksu et al., 2008;  
189 İşler, 2012; İşler et al., 2016), with a Nisyros tephra in southern Aegean Sea core MC27 (301-  
190 307 cm depth; Vinci, 1983, 1985), and with the ML3 and ML4 layers in the lacustrine core  
191 ML01 from Megali Limni, Lesvos Island, Greece (Margari et al., 2007, 2009) (Figs. 3b-c).  
192 There is only a vague compositional overlap with a proposed Lower Nisyros Pumice tephra in  
193 Adriatic Sea core TRI172-26 (133.1-133.4 cm depth; Hardiman, 1999) (Figs. 3b-c), and the  
194 MT3 glass chemistry is clearly distinct from the andesitic composition of the marine X-1 tephra  
195 in the Aegean Sea (Fig. 3a).

196 Notably, the previous lack of glass chemical data of Nisyros tephra land deposits has for long  
197 prevented reliable tephra correlations for the above-mentioned sites, and, in the case of Megali  
198 Limni, partly confounded the core chronology and therewith the proxy data interpretations.  
199 Hence, the respective tephra datasets of these records have been re-evaluated within this  
200 study to allow for a direct comparison with SoM data (Fig. 4).



202 **Figure 4:** Comparison of palaeoenvironmental records of the last 70 kyr from the Aegean-  
203 Black Sea region by using mutual tephra isochrons (red dotted lines). **a)** Oxygen isotope curve  
204 of planktonic foraminifera from Aegean Sea core MAR03-28 (İşler et al., 2016) with timescale  
205 of Marine Isotope Stages (MIS); XRF-Ca-records of core MRS-CS27 (**b**) and MRS-CS18 (**c**)  
206 from the Sea of Marmara (Çağatay et al., 2019; this study) with positions of wiggle-matched  
207 Greenland Interstadials (GI). **d)** Total tree pollen percentages in the Megali Limni sequence,  
208 Lesvos Island (Margari et al., 2009; Sánchez Goñi et al., 2017) on a revised timescale (this  
209 study; see also Supplement Fig. B2-B4 and Supplement C) and with positions of wiggle-  
210 matched GIs. **e)** Total tree pollen percentages of the Tenaghi Philippon peat sequence,  
211 Southeast Greece (Müller et al., 2011; Wulf et al., 2018); **f)** Oxygen Isotope record of  
212 Greenland ice core NGRIP (NGRIP members, 2004) with positions of Greenland Interstadials  
213 (GI).

214

#### 215 **4.1 Synchronisation with distal terrestrial tephra archives**

216 The comparison of the MT3 tephra data with the tephrostratigraphic record of the lacustrine  
217 record of Megali Limni (Margari et al., 2007, 2009; Pyle and Margari, 2009) is quite complex  
218 and requires a thorough revision of the published dataset. Margari et al. (2007, 2009) identified  
219 six visible tephra layers, namely ML1 to ML6, in core ML01 for which the age of the oldest  
220 tephra ML6 has been interpolated to ~57.6 cal ka BP. The sequence contains two closely-  
221 spaced Nisyros tephra layers, ML3 and ML4 (Margari et al., 2007), with identical glass  
222 composition that is also comparable to that of the UNP proximal deposits (Tomlinson et al.,  
223 2012a) and the SoM MT3 tephra (Fig. 3c-d). The deposition ages of the ML3 and ML4 tephra  
224 layers have been originally extrapolated to ~46.0 and ~46.8 cal ka BP (Margari et al., 2007;  
225 Pyle and Margari, 2009); those, however, are considerably younger than the UNP age  
226 constrained from the SoM sequences in this study.

227 The original age-depth model of the Megali Limni sequence is based on a combination  
228 of tephrochronology and radiocarbon dating (Margari et al., 2007). When reviewing the  
229 tephrochronological dataset, it is apparent that the youngest tephtras ML1 and ML2, correlated  
230 by Margari et al. (2007) with the Y-2/Cape Riva and Y-5/Campanian Ignimbrite eruptions

231 respectively, are reliable time marker for the age-depth model. However, the two oldest  
232 tephra ML5 and ML6 have been miscorrelated, and their imported ages therefore significantly  
233 falsified the chronology. The younger ML5 tephra was previously correlated by Margari et al.  
234 (2007) to the Y-6/Green Tuff of Pantelleria ( $44.1 \pm 0.6$  ka; Scaillet et al., 2013). However, FeO  
235 values of ML5 tephra glasses are too low to justify an assignment to the Y-6 tephra but rather  
236 suggest a correlation with the older Pantelleria P-11 tephra (133 ka; Satow et al., 2015) (Fig.  
237 3d). A correlation with the P-11 tephra has been also postulated by Vogel et al. (2010) and is  
238 strongly supported by the widespread dispersal of this tephra in the Balkan (e.g., Vogel et al.,  
239 2010; Karkanis et al., 2015; Leicher et al., 2016) and southern Aegean Sea (Satow et al.,  
240 2015) regions. The ML6 tephra, on the other hand, has been previously assigned to an  
241 unknown Aegean Arc tephra (Margari et al., 2007) despite its glass composition showing an  
242 unambiguous chemical match with the marine W-3 and the Kos Plateau Tuff (KPT;  $161.3 \pm$   
243  $1.1$  ka, Smith et al., 1996) (Fig. 3b-c). The stratigraphic position below the 133 ka-Pantelleria  
244 tephra and the fact that the KPT is present in marine records from the Aegean-Black Sea  
245 region (e.g., Satow et al., 2015; Wegwerth et al., 2019; Wulf et al., 2020) additionally support  
246 a correlation of ML6 to the W-3/KPT eruption.

247         When considering the tephra ages of the revised ML5/P-11 and ML6/KPT correlations  
248 and re-evaluating the Megali Limni pollen record of Margari et al. (2009) by wiggle-matching  
249 with the Tenaghi Philippon pollen and the Greenland oxygen isotope records (Fig. 4d-f), it is  
250 evident that the basal sediments of the Megali Limni core date back to the penultimate glacial  
251 instead of MIS 4 (Supplement Figs. B2-B4, Supplement C). The new ML01 chronology also  
252 provides revised modelled dates of the ML3 and ML4 tephra at  $55,970 \pm 2040$  cal a BP and  
253  $57,490 \pm 2030$  cal a BP respectively (Fig. 4). The ML4 age at  $\sim 57.5$  cal ka BP in particular  
254 agrees well and within  $2\sigma$  uncertainties with the UNP/MT3 extrapolated age in the SoM  
255 sediments ( $\sim 57.1$  cal ka BP) and with the U-Th disequilibrium zircon date of proximal UNP  
256 deposits at  $\sim 58.4$  ka by Popa et al. (2020). Furthermore, the ML4 tephra stratigraphic position  
257 in the Megali Limni pollen record confirms the occurrence of the UNP eruption at the

258 termination of Greenland Interstadial GI-16 (Fig. 4, Supplement Figs. B3-B4). The revised  
259 chronostratigraphic information in combination with the lack of proximal and marine distal  
260 evidence for more than one UNP eruption suggest that ML4 is most likely the primary tephra  
261 layer in the Megali Limni sequence and that the younger ML3 tephra layer might have been  
262 derived from reworking processes which, however, needs to be further investigated.

263

#### 264 ***4.2 Links with marine tephra archives and UNP dispersal***

265 The majority of Nisyros tephra findings derives from the marine realm. For example, Aksu et  
266 al. (2008) identified the thin 'tephra  $\delta$ ' layer in several sediment cores collected from across  
267 the Aegean Sea and north of Nisyros volcano (MAR-sites in Fig. 1a). Tephra  $\delta$  is  
268 stratigraphically positioned between the Campanian Ignimbrite tephra layer and sapropel S3  
269 and has been dated by extrapolation of the marine oxygen isotope stratigraphy to originally  
270 42-44 ka BP (Aksu et al., 2008). Higher-resolution  $\delta^{18}\text{O}$  records published by İşler et al. (2016)  
271 have corrected this age to 53-58 ka BP, therewith placing tephra  $\delta$  at the onset of MIS 3 (Fig.  
272 4a). A previous correlation of tephra  $\delta$  with the Lower Nisyros Pumice by Aksu et al. (2008)  
273 has been revised to the Upper Nisyros pumices by Tomlinson et al. (2012a), and the new SoM  
274 MT3 dataset corroborates this assignment (Figs. 3b-c). Therewith, the UNP tephra, together  
275 with the Campanian Ignimbrite and the Santorini Y-2, presents an additional valuable  
276 isochrone for the glacial period that allows for detailed palaeoceanographic reconstructions of  
277 the Aegean-Black Sea region (Fig. 4).

278 Other UNP tephra findings in the Aegean Sea include a 6-cm-thick layer in core MC27,  
279 located ~120 km south of Nisyros (Vinci, 1983, 1985). The chronostratigraphic position of the  
280 MC27 tephra is only poorly constrained, hence impeding a direct comparison with the SoM  
281 and other Aegean Sea data. Nevertheless, the MC27 tephra plays an important role for  
282 reconstruction of the UNP tephra dispersal in the Aegean Sea region since its occurrence  
283 indicates an additional southerly dispersion alongside the predominant northerly dispersal

284 pattern as evidenced from the MAR Aegean Sea, Megali Limni, and SoM cores. However,  
285 MC27 is to date the only distal core south of Nisyros containing the UNP tephra, while other  
286 nearby high-resolution tephra archives, i.e. cores LC21 (Satow et al., 2015), KL49 and KL51  
287 (Wulf et al., 2020) lack this tephra (Fig. 1a). Therefore, further investigations are required to  
288 demonstrate the primary character of the MC27 tephra prior to interpret this complex dispersal  
289 pattern.

290

## 291 **5. Conclusions**

292 The new findings of the Upper Nisyros Pumice as MT3 tephra in the Sea of Marmara in  
293 combination with high-resolution proxy datasets provided a new modelled age of the UNP  
294 eruption at  $57.1 \pm 1.5$  cal ka BP. This tephra age confirms the radioisotopic date of the UNP  
295 by Popa et al. (2020) and agrees well with the revised modelled age of the UNP distal tephra  
296 equivalent ML4 in the Megali Limni terrestrial record. The stratigraphic position of the UNP in  
297 palaeoenvironmental records of the Aegean-Black Sea region suggests a deposition at the  
298 termination of Greenland Interstadial GI-16 (SoM, Megali Limni) and at the onset of MIS 3  
299 (Aegean Sea cores).

300 The occurrence of the UNP tephra in the SoM represents to date the furthest finding  
301 in the north-eastern part of the Aegean-Black Sea region, suggesting likely a transport by  
302 strong prevailing southerly winds at the time of the eruption and implying the possibility to  
303 detect this tephra in even more distal positions than previously believed. It is therefore  
304 recommended that future palaeoenvironmental studies in this region implement detailed  
305 (crypto)tephra studies to take advantage of this new tephra isochrone.

306

## 307 **Acknowledgements**

308 We thank the scientific team of Marsite cruise and the captains and crews of RV Pourquoi  
309 pas? for the recovery of cores MRS-CS18 and MRS-CS2. The Marsite cruise was co-funded  
310 by the EC FP7 project MARSITE (grant number: 308417), the “Laboratoire d'Excellence”  
311 LabexMER (ANR-10-LABX-19) through the projects called Micro-GaMa and MISS Marmara,  
312 and by a grant from the French government under the program “Investissements d'Avenir”.  
313 We also thank Mehmet Ali Oral of Geological Engineering Department at ITU, for the  
314 preparation of polished thin sections for tephra EPM analysis.

315

## 316 **References**

- 317 Aksu, A.E., Jenner, G., Hiscott, R.N., Isler, E.B., 2008. Occurrence, stratigraphy and  
318 geochemistry of Late Quaternary tephra layers in the Aegean Sea and the Marmara Sea.  
319 *Mar. Geol.* 252, 174-192. <https://doi.org/10.1016/j.margeo.2008.04.004>
- 320 Albert, P.G., Hardiman, M., Keller, J., Tomlinson, E.L., Smith, V.C., Bourne, A.J., Wulf, S.,  
321 Zanchetta, G., Sulpizio, R., Müller, U.C., Pross, J., Ottolini, L., Matthews, I.P., Blockley,  
322 S.P.E., Menzies, M.A., 2015. Revisiting the Y-3 tephrostratigraphic marker: a new  
323 diagnostic glass geochemistry, age estimate, and details on its climatostratigraphical  
324 context. *Quat. Sci. Rev.* 118, 105-121. <https://doi.org/10.1016/j.quascirev.2014.04.002>
- 325 Allen, S.R., 2001. Reconstruction of a major caldera-forming eruption from pyroclastic  
326 deposit characteristics: Kos Plateau Tuff, eastern Aegean Sea. *J. Volcanol. Geoth. Res.*  
327 105, 141-162. [https://doi.org/10.1016/S0377-0273\(00\)00222-5](https://doi.org/10.1016/S0377-0273(00)00222-5)
- 328 Andersen, K.K., Svensson, A., Johnsen, S., S.O. Rasmussen, S.O., Bigler,  
329 M., Rothlisberger, R., Ruth, U., Siggaard-Andersen, M.L., Steffensen, J.P., Dahl-  
330 Jensen, D., Vinther, B.M., Clausen, H.B., 2006. The Greenland ice core chronology 2005,  
331 15–42 ka. part 1: constructing the time scale. *Quat. Sci. Rev.* 25, 3246-3257.  
332 <https://doi.org/10.1016/j.quascirev.2006.08.002>
- 333 Bachmann, O., Schoene, B., Schnyder, C., Spikings, R., 2010.  $^{40}\text{Ar}/^{39}\text{Ar}$  and U/Pb dating of  
334 young rhyolites in the Kos-Nisyros volcanic complex, Eastern Aegean Arc (Greece): age  
335 discordance due to excess  $^{40}\text{Ar}$  in biotite. *Geochem. Geophys. Geosy.* 11, Q0AA08.  
336 <https://doi.org/10.1029/2010GC003073>



337 Bachmann, O., Deering, C.D., Ruprecht, J.S., Huber, C., Skopelitis, A., Schnyder, C., 2012.  
338 Evolution of silicic magmas in the Kos-Nisyros volcanic center, Greece: a petrological  
339 cycle associated with caldera collapse. *Contrib. Mineral. Petr.* 163, 151-166.  
340 <https://doi.org/10.1007/s00410-011-0663-y>

341 Barberi, F., Navarro, J.M., Rosi, M., Santacroce, R., Sbrana, A., 1988. Explosive interaction  
342 of magma with groundwater: insights from xenoliths and geothermal drillings. *Rend. Soc.*  
343 *Ital. Mineral. Petrol.* 43, 901–926. <http://hdl.handle.net/11568/15177>

344 Bourne, A.J., Albert, P.G., Matthews, I.P., Trincardi, F., Wulf, S., Asioli, A., Blockley, S.P.E.,  
345 Keller, J., Lowe, J.J., 2015. Tephrochronology of core PRAD 1-2 from the Adriatic Sea:  
346 insights into Italian explosive volcanism for the period 200-80 ka. *Quat. Sci. Rev.* 116, 28-  
347 43. <https://doi.org/10.1016/j.quascirev.2015.03.006>

348 Bronk Ramsey, C., 2021. OxCal version 4.4.3. <https://c14.arch.ox.ac.uk/oxcal.html>.

349 Bronk Ramsey, C., Albert, P.G., Blockley, S.P.E., Hardiman, M., Housley, R.A., Lane, C.S.,  
350 Lee, S., Matthews, I.P., Smith, V.C., Lowe, J.J., 2015. Improved age estimates for key  
351 Late Quaternary European tephra horizons in the RESET lattice. *Quat. Sci. Rev.* 118, 18-  
352 32. <https://doi.org/10.1016/j.quascirev.2014.11.007>

353 Çağatay, M.N., Wulf, S., Sancar, Ü., Özmaral, A., Vidal, L., Henry, P., Appelt, O., Gasperini,  
354 L., 2015. The tephra record from the Sea of Marmara for the last ca. 70 ka and its  
355 palaeoceanographic implications. *Mar. Geol.* 361, 96-110.  
356 <https://doi.org/10.1016/j.margeo.2015.01.005>

357 Çağatay, M.N., Eriş, K.K., Makaroğlu, Ö., Yakupoğlu, N., Henry, P., Leroy, S.A.G., Uçarkuş,  
358 G., Sakıncı, M., Yalamaz, B., Bozyiğit, C., Kende, J., 2019. The Sea of Marmara during  
359 Marine Isotope Stages 5 and 6. *Quat. Sci. Rev.* 220, 124-141.  
360 <https://doi.org/10.1016/j.quascirev.2019.07.031>

361 Di Paola, G.M., 1974. Volcanology and petrology of Nisyros Island (Dodecanese, Greece). *B.*  
362 *Volcanol.* 38, 944-987. <https://doi.org/10.1007/BF02597100>

363 Druitt, T.H., Edwards, L., Mellors, R.M., Pyle, D.M., Sparks, R.S.J., Lanphere, M., Davies,  
364 M., Barriero, B., 1999. Santorini Volcano. *Geol. Soc. Spec. Publ.* 19, 165 pp.

365 Fabbro, G.N., Druitt, T.H., Scaillet, S., 2013. Evolution of the crustal magma plumbing  
366 system during the build-up to the 22-ka caldera-forming eruption of Santorini (Greece). *B.*  
367 *Volcanol.* 75, 767. <https://doi.org/10.1007/s00445-013-0767-5>

368 Giaccio, B., Nomade, S., Wulf, S., Isaia, R., Sottili, G., Cavuoto, G., Galli, P., Messina, P.,  
369 Sposato, A., Sulpizio, R., Zanchetta, G., 2012. The late MIS 5 Mediterranean tephra  
370 markers: a reappraisal from peninsular Italy terrestrial records. *Quat. Sci. Rev.* 56, 31-45.  
371 <https://doi.org/10.1016/j.quascirev.2012.09.009>

372 Giaccio, B., Hajdas, I., Isaia, R., Deino, A., Nomade, S., 2017. High-precision  $^{14}\text{C}$  and  $^{40}\text{Ar}/^{39}\text{Ar}$   
373 dating of the Campanian Ignimbrite (Y-5) reconciles the time-scale of climatic cultural  
374 processes at 40 ka. *Sci. Rep.* 7, 45940. <https://doi.org/10.1038/srep45940>

375 Giaccio, B., Leicher, N., Mannella, G., Monaco, L., Regattieri, E., Wagner, B., Zanchetta, G.,  
376 Gaeta, M., Marra, F., Nomade, S., Palladino, D.M., Pereira, A., Scheidt, S., Sottili, G.,  
377 Wonik, T., Wulf, S., Zeeden, C., Aristegui, D., Cavinato, G.P., Dean, J.R., Florindo, F.,  
378 Leng, M., Macrì, P., Niespolo, E., Renne, P.R., Rolf, C., Sadori, L., Thomas, C., Tzedakis,  
379 P.C., 2019. Extending the tephra and palaeoenvironmental record of the Central  
380 Mediterranean back to 430 ka: a new core from Fucino Basin, central Italy. *Quat. Sci.*  
381 *Rev.* 225, 106003. <https://doi.org/10.1016/j.quascirev.2019.106003>

382 Hardiman, J.C., 1999. Deep sea tephra from Nisyros Island, eastern Aegean Sea, Greece.  
383 *Geol. Soc. Spec. Publ.* 161, 69–88. <https://doi.org/10.1144/GSL.SP.1999.161.01.06>

384 Hunt, J.B., Hill, P.G., 1996. An inter-laboratory comparison of the electron probe  
385 microanalysis of glass geochemistry. *Quatern. Int.* 34-36, 229-241.  
386 [https://doi.org/10.1016/1040-6182\(95\)00088-7](https://doi.org/10.1016/1040-6182(95)00088-7)

387 İşler, E.B., 2012. Paleooceanographic and paleoclimatic evolution of the Aegean Sea since  
388 the last Interglacial (~130 ka BP) with special emphasis on sapropel formation. PhD  
389 Thesis, Memorial University of Newfoundland.  
390 <http://research.library.mun.ca/id/eprint/12114>

391 İşler, E.B., Hiscott, R.N., Aksu, A.E., 2016. Late Quaternary chronostratigraphy of the  
392 Aegean Sea sediments: special reference to the ages of sapropels S1-S5. *Turk. J. Earth*  
393 *Sci.* 25, 1-18. <https://doi.org/10.3906/yer-1501-37>

394 Jochum, K.P., Stoll, B., Herwig, K., Willbold, M., Hofmann, A.W., et al., 2006. MPI-DING  
395 reference glasses for in situ microanalysis: New reference values for element  
396 concentrations and isotope ratios. *Geochem. Geophys. Geosy.* 7(2), Q02008.  
397 <https://doi.org/10.1029/2005GC001060>

398 Karkanas, P., White, D., Lane, C.S., Stringer, C., Davies, W., Cullen, V.L., Smith, V.C.,  
399 Ntinou, M., Tsartsidou, G., Kyparissi-Apostolika, N., 2015. Tephra correlations and  
400 climatic events between the MIS6/5 transition and the beginning of MIS3 in Theopetra  
401 Cave, central Greece. *Quat. Sci. Rev.* 118, 170–181.  
402 <https://doi.org/10.1016/j.quascirev.2014.05.027>

403 Keller, J., Ryan, W.B.F., Ninkovich, D., Altherr, R., 1978. Explosive volcanic activity in the  
404 Mediterranean over the past 200,000 yr as recorded in deep-sea sediments. *Geol. Soc.*  
405 *Am. Bull.* 89, 591-604. [https://doi.org/10.1130/0016-7606\(1978\)89%3C591:EVAITM%3E2.0.CO;2](https://doi.org/10.1130/0016-7606(1978)89%3C591:EVAITM%3E2.0.CO;2)

406  
407 Kuehn, S.C., Froese, D.G., Shane, P.A.R., INTAV Intercomparison Participants, 2011. The  
408 INTAV intercomparison of electron-beam microanalysis of glass by tephrochronology

409 laboratories: Results and recommendations. *Quatern. Int.* 246, 19-47.  
410 <https://doi.org/10.1016/j.quaint.2011.08.022>

411 Kwiecien, O., Arz, H.W., Lamy, F., Wulf, S., Bahr, A., Röhl, U., Haug, G.H., 2008. Estimated  
412 reservoir ages of the Black Sea since the last glacial. *Radiocarbon* 50(1), 99-118.  
413 <https://doi.org/10.1017/S0033822200043393>

414 Leicher, N., Zanchetta, G., Sulpizio, R., Giaccio, B., Wagner, B., Nomade, S., Francke, A.,  
415 Del Carlo, P., 2016. First tephrostratigraphic results of the DEEP site record from Lake  
416 Ohrid (Macedonia and Albania). *Biogeosciences* 13, 2151-2178.  
417 <https://doi.org/10.5194/bg-13-2151-2016>

418 Limburg, E.M., Varekamp, J.C., 1991. Young pumice deposits on Nisyros, Greece. *B.*  
419 *Volcanol.* 54(1), 68–77. <https://doi.org/10.1007/BF00278207>

420 Longchamp, C., Bonadonna, C., Bachmann, O., Skopelitis, A., 2011. Characterization of  
421 tephra deposits with limited exposure: the example of the two largest explosive eruptions  
422 at Nisyros volcano (Greece). *B. Volcanol.* 73, 1337-1352. [https://doi.org/10.1007/s00445-](https://doi.org/10.1007/s00445-011-0469-9)  
423 [011-0469-9](https://doi.org/10.1007/s00445-011-0469-9)

424 Lowe, D.J., 2011. Tephrochronology and its application: A review. *Quat. Geochronol.* 6, 107-  
425 153. <https://doi.org/10.1016/j.quageo.2010.08.003>

426 Margari, V., Pyle, D.M., Bryant, C., Gibbard, P.L., 2007. Mediterranean tephra stratigraphy  
427 revisited: Results from a long terrestrial sequence on Lesbos Island, Greece. *J. Volcanol.*  
428 *Geoth. Res.* 163, 34-54. <https://doi.org/10.1016/j.jvolgeores.2007.02.002>

429 Margari, V., Gibbard, P.L., Bryant, C.L., Tzedakis, P.C., 2009. Character of vegetational and  
430 environmental changes in southern Europe during the last glacial period; evidence from  
431 Lesbos Island, Greece. *Quat. Sci. Rev.* 28, 1317-1339.  
432 <https://doi.org/10.1016/j.quascirev.2009.01.008>

433 Martin-Puertas, C., Brauer, A., Wulf, S., Ott, F., Lauterbach, S., Dulski, P., 2014. Annual  
434 proxy data from Lago Grande di Monticchio (southern Italy) between 76 and 112 ka: new  
435 chronological constraints and insights on abrupt climatic oscillations. *Clim. Past* 10, 2099-  
436 2114. <https://doi.org/10.5194/cp-10-2099-2014>

437 Milner, A.M., Roucoux, K.H., Collier, R.E.L., Müller, U.C., Pross, J., Tzedakis, P.C., 2016.  
438 Vegetation responses to abrupt climatic changes during the Last Interglacial Complex  
439 (Marine Isotope Stage 5) at Tenaghi Philippon, NE Greece. *Quat. Sci. Rev.* 154, 169-181.  
440 <https://doi.org/10.1016/j.quascirev.2016.10.016>

441 Müller, U.C., Pross, J., Tzedakis, P.C., Gamble, C., Kotthoff, U., Schmiedl, G., Wulf, S.,  
442 Christanis, K., 2011. The role of climate in the spread of modern humans into Europe.  
443 *Quat. Sci. Rev.* 30, 273-279. <https://doi.org/10.1016/j.quascirev.2010.11.016>

444 Narcisi, B., Vezzoli, L., 1999. Quaternary stratigraphy of distal tephra layers in the  
445 Mediterranean - an overview. *Global Planet. Change* 21, 31-50.  
446 [https://doi.org/10.1016/S0921-8181\(99\)00006-5](https://doi.org/10.1016/S0921-8181(99)00006-5)

447 NGRIP members, 2004. High-resolution record of Northern Hemisphere climate extending  
448 into the last interglacial period. *Nature* 431, 147-151. <https://doi.org/10.1038/nature02805>

449 Pe-Piper, G., Moulton, B., 2008. Magma evolution in the Pliocene-Pleistocene succession of  
450 Kos, South Aegean arc (Greece). *Lithos* 106(1–2), 110–124.  
451 <https://doi.org/10.1016/j.lithos.2008.07.002>

452 Popa, R.-G., Guillong, M., Bachmann, O., Szymanowski, D., Ellis, B., 2020. U-Th zircon  
453 dating reveals a correlation between eruptive styles and repose periods at the Nisyros-  
454 Yali volcanic area, Greece. *Chem. Geol.* 555, 11930.  
455 <https://doi.org/10.1016/j.chemgeo.2020.119830>

456 Pyle, D.M., Margari, V., 2009. Reply: Correlation of a widespread Pleistocene tephra marker  
457 from the Nisyros-Yali volcanic complex, Greece. *J. Volcanol. Geoth. Res.* 181, 251-254.  
458 <https://doi.org/10.1016/j.jvolgeores.2008.11.033>

459 Rehren, T., 1988. *Geochemie und Petrologie von Nisyros (Ostliche Agais)*. PhD thesis,  
460 University of Freiburg, pp. 167.

461 Reimer, P.J., Austin, W.E.N., Bard, E., Bayliss, A., Blackwell, P.G., Bronk Ramsey, C.,  
462 Butzin, M., Cheng, H., Edwards, R.L., Friedrich, M., Grootes, P.M., Guilderson, T.P.,  
463 Hajdas, I., Heaton, T.J., Hogg, A.G., Hughen, K.A., Kromer, B., Manning, S.W.,  
464 Muscheler, R., Palmer, J.G., Pearson, C., van der Plicht, J., Reimer, R.W., Richards,  
465 D.A., Scott, E.M., Southon, J.R., Turney, C.S. M., Wacker, L., Adolphi, F., Büntgen, U.,  
466 Capano, M., Fahrni, S.M., Fogtmann-Schulz, A., Friedrich, R., Köhler, P., Kudsk, S.,  
467 Miyake, F., Olsen, J., Reinig, F., Sakamoto, M., Sookdeo, A., Talamo, S., 2020. The  
468 IntCal20 Northern Hemisphere Radiocarbon Age Calibration Curve (0–55 cal kBP).  
469 *Radiocarbon* 62(4), 725–757. <https://doi.org/10.1017/RDC.2020.41>

470 Sánchez Goñi, M.F., Desprat, S., Daniau, A.-L., Bassinot, F.C., Polanco-Martínez, J.M.,  
471 Harrison, S.P., Allen, J.R.M., Anderson, R.S., Behling, H., Bonnefille, R., Burjachs, F.,  
472 Carrión, J.S., Cheddadi, R., Clark, J.S., Combourieu-Nebout, N., Courtney-Mustaphi,  
473 C.J., Debussk, G.H., Dupont, L.M., Finch, J.M., Fletcher, W.J., Giardini, M., González, C.,  
474 Gosling, W.D., Grigg, L.D., Grimm, E.C., Hayashi, R., Helmens, K., Heusser, L.E., Hill, T.,  
475 Hope, G., Huntley, B., Igarashi, Y., Irino, T., Jacobs, B., Jiménez-Moreno, G., Kawai, S.,  
476 Kershaw, P., Kumon, F., Lawson, I.T., Ledru, M.-P., Lezine, A.-M., Liew, P.M., Magri, D.,  
477 Marchant, R., Margari, V., Mayle, F.E., McKenzie, M., Moss, P., Müller, S., Müller, U.C.,  
478 Naughton, F., Newnham, R.M., Oba, T., Pérez-Obiol, R., Pini, R., Ravazzi, C., Roucoux,  
479 K.H., Rucina, S.M., Scott, L., Takahara, H., Tzedakis, P.C., Urrego, D.H., van Geel, B.,  
480 Valencia, B.G., Vandergoes, M.J., Vincens, A., Whitlock, C.L., Willard, D.A., Yamamoto,

481 M., 2017. The ACER pollen and charcoal database: a global resource to document  
482 vegetation and fire response to abrupt climate changes during the last glacial period.  
483 Earth Syst. Sci. Data 9 (2), 679-695. <https://doi.org/10.5194/essd-2017-4>.

484 Satow, C., Tomlinson, E.L., Grant, K.M., Albert, P.G., Smith, V.C., Manning, C.J., Ottolini, L.,  
485 Wulf, S., Rohling, E.J., Lowe, J.J., Blockley, S.P.E., Menzies, M.A., 2015. A new  
486 contribution to the Late Quaternary tephrostratigraphy of the Mediterranean: Aegean Sea  
487 core LC21. Quat. Sci. Rev. 117, 96-112. <https://doi.org/10.1016/j.quascirev.2015.04.005>

488 Satow, C., Grant, K., Wulf, S., Schulz, H., Mallon, A., Matthews, I, Lowe, J., 2020. Detection  
489 and characterisation of Eemian marine tephra layers within the sapropel S5 sediments of  
490 the Aegean and Levantine Seas. Quaternary 3(1), 6. <https://doi.org/10.3390/quat3010006>

491 Scaillet, S., Vita-Scaillet, G., Rotolo, S.G., 2013. Millennial-scale phase relationships  
492 between ice-core and Mediterranean marine records: insights from high-precision  
493  $^{40}\text{Ar}/^{39}\text{Ar}$  dating of the Green Tuff of Pantelleria, Sicily Strait. Quat. Sci. Rev. 78, 141-154.  
494 <https://doi.org/10.1016/j.quascirev.2013.08.008>

495 Smith, P.E., York, D., Chen, Y., Evensen, N.M., 1996. Single crystal  $^{40}\text{Ar}$ - $^{39}\text{Ar}$  dating of a  
496 Late Quaternary paroxysm on Kos, Greece: Concordance of terrestrial and marine ages.  
497 Geophys. Res. Lett. 23, 3047-3050. <https://doi.org/10.1029/96GL02759>

498 Svensson, A., Andersen, K.K., Bigler, M., Clausen, H.B., Dahl-Jensen, D., Davies, S.M.,  
499 Johnsen, S.J., Muscheler, R., Rasmussen, S.O., Röthlisberger, R., Steffensen, J.P.,  
500 Vinther, B.M., 2006. The Greenland Ice Core Chronology 2005, 15-42 ka. Part 2:  
501 comparison to other records. Quat. Sci. Rev. 25, 3258-3267.  
502 <https://doi.org/10.1016/j.quascirev.2006.08.003>

503 Svensson, A., Andersen, K.K., Bigler, M., Clausen, H.B., Dahl-Jensen, D., Davies, S.M.,  
504 Johnsen, S.J., Muscheler, R., Parrenin, F., Rasmussen, S.O., Röthlisberger, R.,  
505 Seierstad, I., Steffensen, J.P., Vinther, B.M., 2008. A 60000-year Greenland stratigraphic  
506 ice core chronology. Clim. Past 4, 47-57. <https://doi.org/10.5194/cp-4-47-2008>

507 Tomlinson, E.L., Kinvig, H.S., Smith, V.C., Blundy, J.D., Gottsmann, J., Müller, W., Menzies,  
508 M.A., 2012a. The Upper and Lower Nisyros Pumices: revisions to the Mediterranean  
509 tephrostratigraphic record based on micron-beam glass geochemistry. J. Volcanol.  
510 Geoth. Res. 243-244, 69–80. <https://doi.org/10.1016/j.jvolgeores.2012.07.004>

511 Tomlinson, E.L., Arienzo, I., Civetta, L., Wulf, S., Smith, V.C., Hardiman, M., Lane, C.S.,  
512 Carandente, A., Orsi, G., Rosi, M., Muller, W., Menzies, M.A., 2012b. Geochemistry of the  
513 Phlegraean Fields (Italy) proximal sources for major Mediterranean tephras: Implications  
514 for the dispersal of Plinian and co-ignimbritic components of explosive eruptions.  
515 Geochim. Cosmochim. Ac. 93, 102-128. <https://doi.org/10.1016/j.gca.2012.05.043>

516 Tomlinson, E.L., Smith, V.C., Albert, P.G., Aydar, E., Civetta, L., Cioni, R., Çubukçu, E.,  
517 Gertisser, R., Isaia, R., Menzies, M.A., Orsi, G., Rosi, M., Zanchetta, G., 2015. The major

518 and trace element glass compositions of the productive Mediterranean volcanic sources:  
519 tools for correlating distal tephra layers in and around Europe. *Quat. Sci. Rev.* 118, 48-66.  
520 <https://doi.org/10.1016/j.quascirev.2014.10.028>

521 Vakhrameeva, P., Koutsodendris, A., Wulf, S., Fletcher, W.J., Appelt, O., Knipping, M.,  
522 Gertisser, R., Trieloff, M., Pross, J., 2018. The cryptotephra record of the Marine Isotope  
523 Stage 12 to 10 interval (460-335 ka) at Tenaghi Philippon, Greece: Exploring  
524 chronological markers for the Middle Pleistocene of the Mediterranean region. *Quat. Sci.*  
525 *Rev.* 200, 313–333. <https://doi.org/10.1016/j.quascirev.2018.09.019>

526 Vakhrameeva, P., Wulf, S., Koutsodendris, A., Tjallingii, R., Fletcher, W.J., Appelt, O.,  
527 Ludwig, T., Knipping, M., Trieloff, M., Pross, J., 2019. Eastern Mediterranean volcanism  
528 during Marine Isotope Stages 9 to 7e (335–235 ka): Insights based on cryptotephra  
529 layers at Tenaghi Philippon, Greece. *J. Volcanol. Geoth. Res.* 380, 31–47.  
530 <https://doi.org/10.1016/j.jvolgeores.2019.05.016>

531 Vinci, A., 1983. A new ash layer ‘Nisyros Layer’ in the Aegean Sea sediments. *Bollettino di*  
532 *Oceanologia Teorica ed Applicata* 1, 341–342.

533 Vinci, A., 1985. Distribution and chemical composition of tephra layers from Eastern  
534 Mediterranean abyssal sediments. *Mar. Geol.* 64, 143-155. [https://doi.org/10.1016/0025-](https://doi.org/10.1016/0025-3227(85)90165-3)  
535 [3227\(85\)90165-3](https://doi.org/10.1016/0025-3227(85)90165-3)

536 Vogel, H., Wagner, B., Zanchetta, G., Sulpizio, R., Rosén, P., 2010. A Paleoclimate record  
537 with tephrochronological age control for the last glacial-interglacial cycle from lake Ohrid,  
538 Albania and Macedonia. *J. Paleolimnol.* 44, 295-310. [https://doi.org/10.1007/s10933-009-](https://doi.org/10.1007/s10933-009-9404-x)  
539 [9404-x](https://doi.org/10.1007/s10933-009-9404-x)

540 Wegwerth, A., Dellwig, O., Wulf, S., Plessen, B., Kleinhanns, I.C., Nowaczyk, N.C., Jiabo, L.,  
541 Arz, H.W., 2019. Major hydrological shifts in the Black Sea “Lake” in response to ice  
542 sheet collapses during MIS 6 (130-184 ka BP). *Quat. Sci. Rev.* 219, 126-144.  
543 <https://doi.org/10.1016/j.quascirev.2019.07.008>

544 Wolff, E.W., Chappellaz, J., Blunier, T., Rasmussen, S.O., Svensson, A., 2010. Millennial-  
545 scale variability during the last glacial: The ice core record. *Quat. Sci. Rev.* 29, 2828-  
546 2838. <https://doi.org/10.1016/j.quascirev.2009.10.013>

547 Wulf, S., Keller, J., Paterne, M., Mingram, J., Lauterbach, S., Opitz, S., Sottili, G., Giaccio,  
548 B., Albert, P.G., Satow, C., Tomlinson, E.L., Viccaro, M., Brauer, A., 2012. The 100-133  
549 ka record of Italian explosive volcanism and revised tephrochronology of Lago Grande di  
550 Monticchio. *Quat. Sci. Rev.* 58, 104–123. <https://doi.org/10.1016/j.quascirev.2012.10.020>

551 Wulf, S., Hardiman, M., Staff, R.A., Koutsodendris, A., Appelt, O., Blockley, S.P.E., Lowe,  
552 J.J., Manning, C.J., Ottoloni, L., Schmitt, A.K., Smith, V.C., Tomlinson,  
553 E.L., Vakhrameeva, P., Knipping, M., Kotthoff, U., Milner, A.M., Müller, U.C., Christanis,  
554 K., Kalaitzidis, S., Tzedakis, C., Schmiedl, G., Pross, J., 2018. The Marine Isotope Stage



555 1 to 5 cryptotephra record of Tenaghi Philippon, Greece: Towards a detailed  
556 tephrostratigraphic framework for the Eastern Mediterranean region. *Quat. Sci. Rev.* 186,  
557 236-262. <https://doi.org/10.1016/j.quascirev.2018.03.011>

558 Wulf, S., Keller, J., Satow, C., Gertisser, R., Kraml, M., Grant, K.M., Appelt, O.,  
559 Vakhrameeva, P., Koutsodendris, A., Hardiman, M., Schulz, H., Pross, J.,  
560 2020. Advancing Santorini's tephrostratigraphy: new glass geochemical data and  
561 improved marine-terrestrial tephra correlations for the past ~360 kyrs. *Earth-Sci.*  
562 *Rev.* 200, 102964. <https://doi.org/10.1016/j.earscirev.2019.102964>

563

564 **Supplement A:** *EPMA glass data of tephra layers MT-1, MT-2 and MT-3 from cores MRS-*  
565 *CS18 and MRS-CS27; EPMA glass reference data for data control; Bayesian age models of*  
566 *cores MRS-CS18 and MRS-CS27.*

567 **Supplement Table B1:** *Revised age constraints (radiocarbon, tephra) of Sea of Marmara*  
568 *sediment cores MRS-CS18 and MRS-CS27.*

569 **Supplement Figure B1:** *OxCal age-depth models of cores MRS-CS18 and MRS-CS27.*

570 **Supplement Figure B2:** *Comparison of original and revised age-depth models of Megali*  
571 *Limni core ML01.*

572 **Supplement Figure B3:** *Selected pollen taxa (Total tree taxa, Juniper+Pinus, and Artemisia)*  
573 *of the ML01 sequence from Megali Limni on a depth scale.*

574 **Supplement Figure B4:** *Selected pollen taxa (Total tree taxa, Juniper+Pinus, and Artemisia)*  
575 *of the ML01 sequence from Megali Limni on a revised time scale (this study).*

576 **Supplement C:** *Revised age constraints and Bayesian age model of Megali Limni core*  
577 *ML01 (this study); ML01 pollen dataset from Margari et al. (2009) and Sánchez Goñi et al.*  
578 *(2017) on a revised timescale; Age constraints used for the original ML01 chronology of*  
579 *Margari et al. (2007, 2009).*